https://doi.org/10.33263/BioMed22.093104

ISSN: 2668-6007 https://biomedicalengineering.international

Biomedical Engineering International

Volume 2, Issue 2, Pages 0093-0104
2020

Article

Received: 07.05.2020
Accepted: 31.05.2020
Published: 04.06.2020

Characterization of drug-loaded unmodified and MgO-modified mesoporous silicas

Takuya Ehiro [1,*]

[1] Osaka Research Institute of Industrial Science and Technology, Ayumino 2-7-1, Izumi-shi, Osaka 594-1157, Japan;
* Correspondence: ehirot@tri-osaka.jp; Scopus ID: 56523205600

Abstract: In this study, unmodified and MgO-modified mesoporous silicas were prepared under mild conditions, without hydrothermal treatment. The obtained mesoporous materials were utilized as ibuprofen (IB) carrier. IB was loaded onto mesoporous materials using three methods: (1) adsorption, (2) impregnation, and (3) physical mixing. Mesoporous materials with or without IB were evaluated by various techniques such as thermogravimetry differential thermal analysis (TG-DTA), X-ray diffraction (XRD) analysis, scanning electron microscopy (SEM), N_2 adsorption-desorption measurements, CO_2 temperature-programmed desorption, Fourier transform infrared spectroscopy (FT-IR), and terahertz time-domain spectroscopy (THz-TDS). MgO modification improved the solid basicity of unmodified mesoporous silicas and their IB adsorption capacity. In addition, MgO modification and IB loading method influenced the physical and chemical properties of IB. The impregnation and physical mixing methods could give similar physical and chemical states to pure IB, while the adsorption method may have been favorable for IB dispersion on the surface. Moreover, the absorption band shifts in the FT-IR spectra suggested that the carboxylic acid group of IB interacted with the basic MgO-modified surface. Since the results of THz-TDS roughly correlated with those of XRD and FT-IR, it was suggested that THz-TDS spectroscopy could be a rapid and non-destructive tool to investigate various drug delivery systems.

Keywords: drug carrier, ibuprofen, mesoporous silica, solid basicity, terahertz time-domain spectroscopy.

1. Introduction

Highly bioavailable drugs easily reach systemic circulation when orally administered. Therefore, oral drug delivery is one of the most common methods for administration because it is safe and void of pain. However, only a small portion of poorly water-soluble drugs reach organs. Moreover, burst release of a drug leads to a rapid change in blood drug concentration. To overcome disadvantages of the conventional drug dosage forms, controlled drug delivery systems (DDSs) have been studied extensively [1].

To date, polymeric, lipid, inorganic, and metal-containing drug carriers have been developed to control drug release. Among them, mesoporous silicas are promising materials for controlling and maintaining drug release owing to the following advantages: (1) easy synthesis, (2) tunable pore and particle size, (3) efficient and simple functionalization, (4) high specific surface area, (5)

Cite This Article: Ehiro, T. Characterization of drug-loaded unmodified and MgO-modified mesoporous silicas. Biomed Eng Int **2020**, 2, 0093-0104. https://doi.org/10.33263/BioMed22.093104

large pore volume adequate for high drug loading, (6) ability to enhance oral drug bioavailability, and (7) ability to stabilize a drug [1].

In this study, Santa Barbara Amorphous-15 (SBA-15), mesoporous silica with a 2D hexagonally ordered mesoporous structure [2], was utilized as a drug carrier. SBA-15 has high chemical and thermal stability, a great pore wall thickness, and uniform mesopore diameter, which is larger than those of Mobil Composition Matter (MCM) type mesoporous silicas such as MCM-41 and MCM-48 [3]. These features make SBA-15 suitable for adsorption of a large molecule and surface modification. Hence, SBA-15 use in DDSs has attracted much attention in recent years, as reviewed by Vavsari et al. [4].

However, surfaces of mesoporous silicas, including SBA-15, are chemically inert. Therefore, their surfaces often interact weakly with drug molecules, resulting in low adsorption capacity and rapid drug release. To improve the controlled release abilities, surface functionalization is effective. In this study, SBA-15 was modified with MgO to enhance its solid basicity and interaction between surface and acidic drug molecules. MgO modification of mesoporous silicas lowers drug release rates and/or enhances drug adsorption capacities [3,5,6]. In addition to DDSs, MgO-modified mesoporous silicas can be used as catalysts [7,8], catalyst supports [9–14], adsorbents [15,16], and humidity sensors [17,18].

Conventionally, MgO/SBA-15 was prepared by stirring precursor solutions, containing Si and Mg, at 313 K for 24 h and aging them at 373 K for 24 or 48 h [3,5,12,14,16,17,19,20]. We prepared MgO/SBA-15 more rapidly at a lower temperature to save energy and preparation time [21]. In this study, MgO/SBA-15 prepared by the facile synthesis method was utilized as a carrier for ibuprofen (IB), which is currently used in a range of pharmaceutical formulations as an analgesic and anti-inflammatory drug [22]. Therefore, it is important to understand the fundamental physical and chemical properties of IB-loaded inorganic drug carriers because cross-referencing studies on drug carriers, including mesoporous silica, can facilitate DDS technology development by giving a broader picture.

In this study, IB-loaded materials were characterized using various techniques such as thermogravimetry–differential thermal analysis (TG-DTA), X-ray diffraction (XRD) analysis, scanning electron microscopy (SEM), N_2 adsorption-desorption measurement, CO_2 temperature-programmed desorption (CO_2-TPD), Fourier transform infrared spectroscopy (FT-IR), and terahertz time-domain spectroscopy (THz-TDS). Although THz-TDS is reportedly a non-destructive and non-contact testing tool, fundamental THz-TDS-related data on drug-loaded inorganic materials are insufficient. Herein, MgO/SBA-15s, on which IB was loaded using three different methods: [(1) adsorption, (2) impregnation, and (3) physical mixing] were evaluated using the THz-TDS technique. The IB loading methods were found to influence IB physical and chemical properties. Moreover, the THz-TDS spectra changed, depending on the loading method and solid basicity. Sensitivity to IB in the THz-TDS measurements decreased by modifying SBA-15 with MgO.

2. Materials and Methods

2.1. Materials

Tetraethoxysilane [$(C_2H_5O)_4Si$; TEOS, 98%], magnesium acetate tetrahydrate [$Mg(OAc)_2{\cdot}4H_2O$, 99%], and potassium bromide (KBr, 99%) were purchased from Fujifilm Wako Pure Chemical Corporation. Hydrochloric acid (HCl, 35%) and n-hexane (96 %) were purchased from Kishida Chemical Co., Ltd. Poly(ethylene glycol)-block-poly(propylene glycol)-block-poly(ethylene glycol) (P123; PEO_{20}-PPO_{70}-PEO_{20}, average molecular weight ~5800) was purchased from Sigma-Aldrich Japan, Inc. IB (98 %) was purchased from Tokyo Chemical Industry Co., Ltd. All chemicals were used as received without further purification.

2.2. Synthesis of drug carriers

SBA-15 and MgO/SBA-15 were prepared as previously reported [21,23]. First, 6.0 g of P123 was dissolved in 180 g of 2 M aqueous HCl. In another vessel, 12.9 g of TEOS and 54.0 g of deionized water were mixed. This solution was added to the 2 M aqueous HCl solution, containing P123. This was then stirred vigorously at 318 K for 1 h. Next, this solution, with a white precipitate, was statically aged at 353 K for 3 h. After 3 h of aging, the mixture was evaporated at 353 K with stirring, air dried, and

calcined at 823 K for 3 h at a heating rate of 1.5 K/min. MgO/SBA-15 was prepared using the same procedure, while a specific $Mg(OAc)_2{\cdot}4H_2O$ amount was added to the 2 M aqueous HCl solution, containing P123. The amount of $Mg(OAc)_2{\cdot}4H_2O$ added was adjusted to obtain 15 wt% of MgO content.

2.3. Drug loading

In this study, IB was loaded by three methods: (1) adsorption, (2) impregnation, and (3) physical mixing. In the adsorption method, 0.4 g of SBA-15 or MgO/SBA-15 was added to 40 ml of n-hexane, containing 0.4 g of IB. To attain adsorption equilibrium, the above slurry was stirred for 48 h at ambient temperature in a closed vessel. The powder was filtered, washed with 40 mL n-hexane, and dried at 313 K for 24 h. The amount of IB adsorbed on the samples was calculated by TG-DTA, as described below. In the impregnation method, 0.4 g of SBA-15 or MgO/SBA-15 was added to 40 ml of n-hexane, containing 0.4 g of IB. Then, the slurry was stirred at ambient temperature in an open vessel until the n-hexane completely evaporated. In the physical mixing method, 0.4 g of SBA-15 or MgO/SBA-15 was physically mixed with IB in an agate mortar to obtain 10 wt%, 30 wt%, or 50 wt% content. The IB-loaded samples obtained by (1) adsorption, (2) impregnation, and (3) physical mixing methods are denoted as (1) IB/SBA-15-ads, IB/MgO/SBA-15-ads, (2) IB/SBA-15-imp, IB/MgO/SBA-15-imp, and (3) IB/SBA-15-phy, and IB/MgO/SBA-15-phy, respectively.

2.4. Characterization

TG-DTAs were performed on a STA7300 (Hitachi High-Technologies Corp.) under 200 mL/min airflow of with a heating rate of 10 K/min from 313 K to 1073 K. XRD patterns were collected on an X-ray diffractometer (SmartLab, Rigaku Corp.) using monochromatized Cu Kα radiation (λ = 0.15418 nm). Morphologies of the materials were observed by SEM (Regulus 8230, Hitachi High-Technologies Corp.). N_2 adsorption-desorption measurements were conducted at 77 K (BELSORP-maxII, Microtrac MRB). Before the measurements, the materials were evacuated at 333 K for 10 h. The Brunauer–Emmett–Teller (BET) surface area and pore size distribution were obtained by analyzing the N_2 adsorption isotherm via BET method [24]. Basic properties of SBA-15 and MgO/SBA-15 were evaluated by CO_2-TPD (BELCAT II, Microtrac MRB). In CO_2-TPD measurements, 0.05 g of each sample was loaded into a quartz tube. Before the measurement, each sample was pretreated with 50 sccm of Ar flow at 773 K for 1 h. Then, each sample was streamed with 50 sccm of 5 % CO_2/Ar for 30 min at 323 K. After the treatment, each sample was treated with 50 sccm of Ar flow for 15 min at 323 K. Then, each sample was heated from 323 K to 1123 K at 10 K/min under 30 sccm of Ar flow. Desorbed CO_2 was monitored using a quadrupole mass spectrometer (BELMass, Microtrac MRB). A fragment peak at m/e = 44 was used to monitor desorbed CO_2. FT-IR spectra were collected using the KBr method and a Vertex 70 (Bruker Corp.). THz-TDS measurements were performed at 297 K on a Tera Prospector (Nippo Precision Co., Ltd.). Before the measurement, each sample was pelletized to form a disc with 15 mm diameter, without a diluting agent such as polyethylene. The optical system was operated in a dry air atmosphere to avoid water absorption signature.

3. Results and Discussion

3.1. TG-DTA

The IB-loaded SBA-15s and MgO/SBA-15s were analyzed using TG-DTA (Figure 1). The DTA curves of pure IB showed two endothermic peaks, as reported previously [25] (Figure 1a). The first endothermic peak could correspond to the melting of IB, although the present melting temperature was slightly higher than that reported previously [3,25]. Additionally, the pure IB TG curve dropped sharply at 423–523 K, indicating rapid weight loss in this temperature region. After loading IB, each sample showed weight loss at a higher temperature (approximately 473–873 K). Considering IB thermal decomposition temperature, amounts of IB/SBA-15-ads and IB/MgO/SBA-15-ads loaded were calculated from the above temperature region. They were determined to be 10 wt% and 30 wt%, respectively, (Figure 1b and f). These results indicated that MgO modification enhanced the IB adsorption capacity of SBA-15. Moreover, the endothermic DTA peaks disappeared in 10 wt% IB/SBA-15-ads and 30 wt% IB/MgO/SBA-15-ads.

This might indicate that low crystallinity IB was dispersed on SBA-15 and MgO/SBA-15 surfaces.

Additionally, exothermic peaks due to IB oxidative decomposition were confirmed after IB adsorption (Figure 1b and f). The DTA exothermic peak of 30 wt% IB/MgO/SBA-15-ads was at a higher temperature than those of 10 wt% IB/SBA-15-ads. This peak shift implied interaction between the MgO-modified surface and IB. The improved IB adsorption capacity could be due to this interaction because IB possesses an acidic carboxyl acid group.

In the impregnation method, the DTA curve of 50 wt% IB/SBA-15-imp showed sharp weight loss and endothermic and exothermic DTA peaks (Figure 1c). These results suggested that 50 wt% IB/SBA-15-imp contained a large amount of IB species, which possessed similar states to pure IB. Contrarily, the 50 wt% IB/MgO/SBA-15-imp endothermic DTA peak was negligible, while the exothermic DTA peaks were confirmed at approximately 573–873 K (Figure 1g). Although low crystallinity IB seemed difficult to disperse on SBA-15 in the impregnation method, 50 wt% IB/MgO/SBA-15-imp showed different thermal behaviors from pure IB and 50 wt% IB/SBA-15-imp (Figure 1a, c, and g).

To compare the adsorption and impregnation methods, 10 wt% and 50 wt% IB/SBA-15-phy, and 30 wt% and 50 wt% IB/MgO/SBA-15-phy were prepared. The endothermic melting DTA peak was not observed for 10 wt% IB/SBA-15-phy, but it was for 50 wt% IB/SBA-15-phy (Figure 1d and e). Therefore, physically mixing a small IB amount with SBA-15 induced interaction between SBA-15 external surface and IB. However, the physical mixing method was insufficient to alter the thermal behavior of a large amount of IB on SBA-15 (Figure 1e).

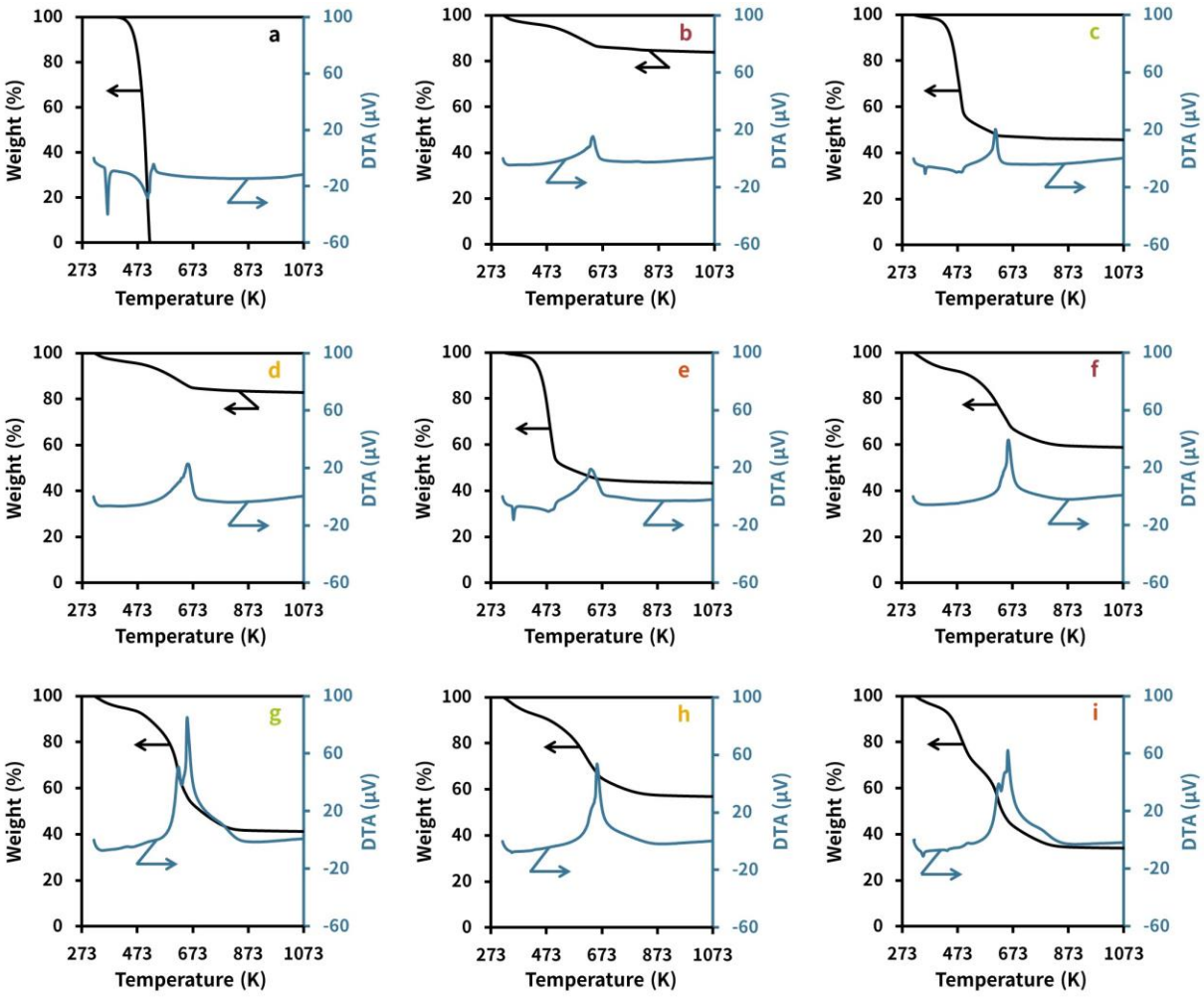

Figure 1. TG-DTA curves of (a) IB, (b) 10 wt% IB/SBA-15-ads, (c) 50 wt% IB/SBA-15-imp, (d) 10 wt% IB/SBA-15-phy, (e) 50 wt% IB/SBA-15-phy, (f) 30 wt% IB/MgO/SBA-15-ads, (g) 50 wt% IB/MgO/SBA-15-imp, (h) 30 wt% IB/MgO/SBA-15-phy, and (i) 50 wt% IB/MgO/SBA-15-phy.

Contrarily, the exothermic DTA peaks of IB/MgO/SBA-15-phy were at a higher temperature than that of IB/SBA-15-phy. These results suggest that the physical mixing method could induce interaction between MgO/SBA-15 and IB, owing to MgO modification. However, it would be difficult to completely alter the thermal behavior of a large amount of IB via the physical mixing method, as Figure 1i shows a two-step weight loss.

3.2. XRD analyses

Figure 2 shows XRD patterns of the unloaded and IB-loaded mesoporous materials. The diffraction peaks at approximately 1–2° are characteristic of SBA-15 (Figure 2b and g). They can be indexed as the (100), (110), and (200) reflections from 2D hexagonally ordered mesostructures, respectively, [5,14,17]. Therefore, the ordered SBA-15 mesostructure did not collapse after MgO modification. These peaks were maintained even after loading IB, regardless of the loading method (Figure 2A and C). Pure IB indicated a diffraction peak at a low angle of ca. 6 °. IB diffraction peaks were also detected at low diffraction angles for 50 wt% IB/SBA-15-imp, 50 wt% IB/SBA-15-phy, 50 wt% IB/MgO/SBA-15-imp, and 50 wt% IB/SBA-15-phy (Figure 2d, f, i, and k). However, 50 wt% IB/MgO/SBA-15-imp diffraction peak shifted from ca. 6 ° to ca. 3.8 °, indicating that the crystal structure of pure IB was changed by the MgO-modified surface.

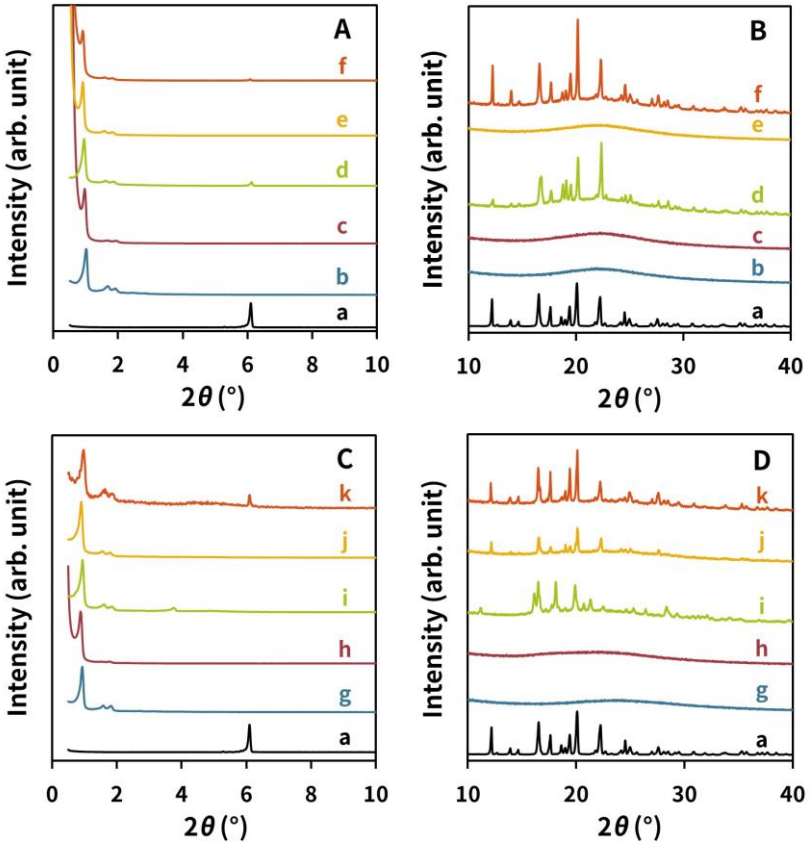

Figure 2. XRD patterns of the various samples at low (A and C) and high (B and D) diffraction angles; (a) IB, (b) SBA-15, (c) 10 wt% IB/SBA-15-ads, (d) 50 wt% IB/SBA-15-imp, (e) 10 wt% IB/SBA-15-phy, (f) 50 wt% IB/SBA-15-phy, (g) MgO/SBA-15, (h) 30 wt% IB/MgO/SBA-15-ads, (i) 50 wt% IB/MgO/SBA-15-imp, (j) 30 wt% IB/MgO/SBA-15-phy, and (k) 50 wt% IB/MgO/SBA-15-phy.

For 50 wt% IB/MgO/SBA-15-imp, diffraction peaks were detected at different high diffraction angles for IB (Figure 2i). Therefore, it was suggested that the MgO-modified surface of MgO/SBA-15 may have changed the IB crystal phase via chemical interactions. Contrarily, this was not confirmed for 50 wt% IB/SBA-15-imp (Figure 2d). The XRD patterns similar to pure IB were detected when a large amount was loaded (Figure 2d, f, j, and k). Unlike the above samples, diffraction peaks at high angles were not detected for 30 wt% IB/MgO/SBA-15-ads (Figure 2h). This XRD pattern suggested that MgO modification promoted IB dispersion. As expected, at low IB content, a no

IB diffraction peak was observed for SBA-15 (Figure 2c and e).

3.3. SEM observations

SBA-15 and MgO/SBA-15 showed rod-like morphologies (Figure 3b and g). After IB adsorption, their morphologies did not change significantly, retaining rod-like units (Figure 3c and h). Contrarily, IB impregnation generated IB and SBA-15 or MgO/SBA-15 aggregates, in addition to the rod-like particles (Figure 3d and i). Therefore, these results indicate that 50 wt% IB impregnation resulted in IB crystallization outside the mesopores to some extent. In the physical mixing method, large aggregates and rod-like particles were observed (Figure 3e, f, j, and k). As shown in Figure 3k, it was hard to distinguish IB and MgO/SBA-15 particles from aggregates in IB/MgO/SBA-15-phy. This might be due to the chemical interaction between IB and MgO/SBA-15.

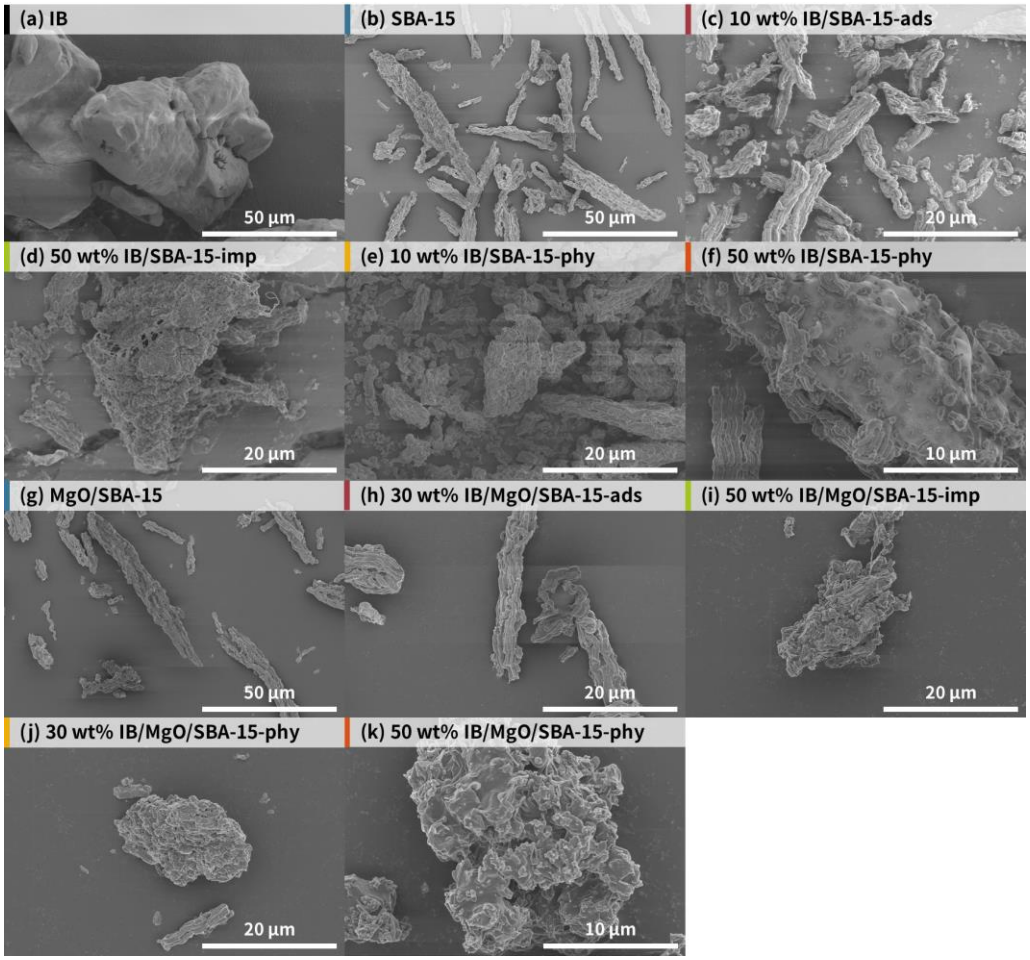

Figure 3. SEM images of the various samples.

3.4. N_2 adsorption-desorption and CO_2-TPD measurements

As shown in Figure 4, SBA-15 and MgO/SBA-15 isotherms were classified as type IV, according to the International Union of Pure and Applied Chemistry (IUPAC) classification. Their isotherms indicated H1 type hysteresis loops, which are characteristics of cylindrical mesopores. Capillary condensations around relative pressure of p/p_0 = 0.7 indicated the mesopores formation with uniform sizes. Hence, it was confirmed that MgO modification did not collapse the ordered SBA-15 mesopores, as confirmed in Figure 2. On the contrary, IB loading decreased N_2 uptakes, specific surface areas, and total pore volumes in all loading methods (Table 1). In the adsorption method, the average SBA-15 and MgO/SBA-15 pore diameters remained unchanged or decreased slightly. It may indicate that IB was adsorbed mainly in their mesopores. On the other hand, considering large aggregate generation in the impregnation and physical mixing methods (Figure 3d–f, i–k), SBA-15 and MgO/SBA-15 could not sufficiently enclose IB in their mesopores using the above methods.

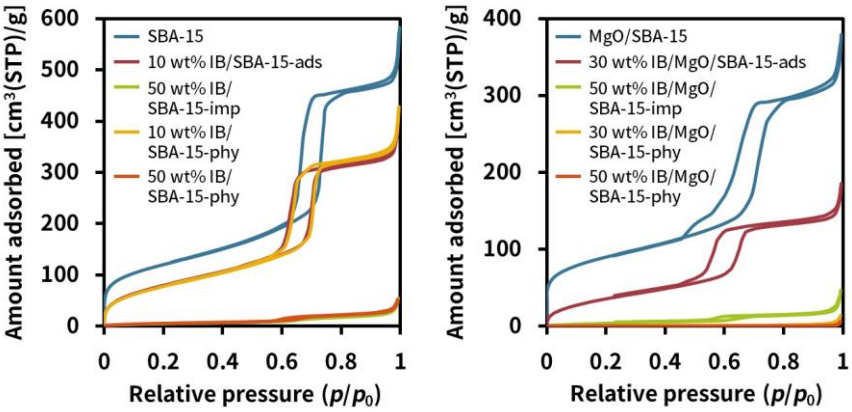

Figure 4. N_2 adsorption-desorption isotherms of the various samples.

Table 1. Physical properties obtained via N_2 adsorption-desorption measurements.

Sample	S_{BET}[a] (m^2/g)	V_{total}[b] (cm^3/g)	d_{av}[c] (nm)
SBA-15	426	0.82	7.7
10 wt% IB/SBA-15-ads	302	0.58	7.7
50 wt% IB/SBA-15-imp	18.5	0.07	16
10 wt% IB/SBA-15-phy	296	0.60	8.2
50 wt% IB/SBA-15-phy	22.1	0.08	14
MgO/SBA-15	321	0.55	7.5
30 wt% IB/MgO/SBA-15-ads	141	0.26	7.4
50 wt% IB/MgO/SBA-15-imp	1.87	0.02	41
30 wt% IB/MgO/SBA-15-phy	16.5	0.07	16
50 wt% IB/MgO/SBA-15-phy	0.40	0.01	78

[a] Specific surface area calculated by BET method.
[b] Total pore volume obtained at the relative pressure of $p/p_0 = 0.99$.
[c] Average pore diameter calculated by $d_{av} = (4V_{total}/S_{BET}) \cdot 10^3$.

To evaluate the basic properties of SBA-15 and MgO/SBA-15, CO_2-TPD measurements were performed (Figure 5). In CO_2-TPD measurements, CO_2 is used as an acidic probe gas to the basic sites of a sample. After CO_2 adsorption on a sample, CO_2 desorption is promoted by heating under an inert gas flow. CO_2 desorption amount and temperature are monitored. Therefore, a large desorption peak area represents a large number of basic sites. Additionally, a high desorption temperature represents strong basicity. SBA-15 did not show an obvious CO_2 desorption peak, indicating that it did not exhibit basicity (Figure 5). Contrarily, MgO/SBA-15 exhibited CO_2 desorption peaks up to a high temperature, despite its lower specific surface area, compared to that of SBA-15 (Table 1). Therefore, MgO modification was found to enhance SBA-15 basicity. This basicity improved SBA-15 IB adsorption capacity from 10 wt% to 30 wt%.

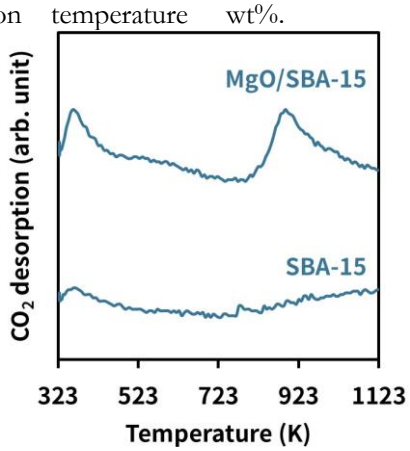

Figure 5. CO_2-TPD spectra of SBA-15 and MgO/SBA-15.

3.5. FT-IR analyses

IB showed a characteristic FT-IR spectrum (Figure 6a). The band at 1720 cm^{-1} might belong to the ν(C=O) stretching vibration, while the weak bands at 1508 and 1462 cm^{-1} to ring vibrations of organic molecules [3]. After 10 wt% IB loading on SBA-15, part of the band due to the carboxyl C=O stretching vibration of pure IB shifted to lower wavenumber (Figure 6b and d). On the contrary, 50 wt% IB loading did not shift significantly (Figure 6c and e). Additional to the physical mixing of SBA-15 with 10 wt% IB, the peak shift was also confirmed by the adsorption method. Therefore, the band shift could be caused not by a mechanochemical effect but by the interaction between SBA-15 and IB. As mentioned above, 50 wt% IB/SBA-15-imp and 50 wt% IB/SBA-15-phy, with slight absorption band shifts, showed the XRD patterns indexed to pure IB (Figure 2B). These results implied that the physical and chemical properties of 50 wt% of IB loaded on SBA-15 were not changed significantly by the impregnation and physical mixing methods.

When loading IB on MgO/SBA-15, a more noticeable band shifted to around 1590 cm^{-1}. It was also observed in the physical mixing method and partial for 50 wt% IB/MgO/SBA-15-phy. Therefore, it may be implied that the external surfaces of the SBA-15 particles, as well as mesopore surfaces, were modified with MgO. The more obvious band shifts after MgO modification suggested a stronger interaction with IB through relatively high basicity (Figure 5), which endows a drug carrier with controlled-release ability [3].

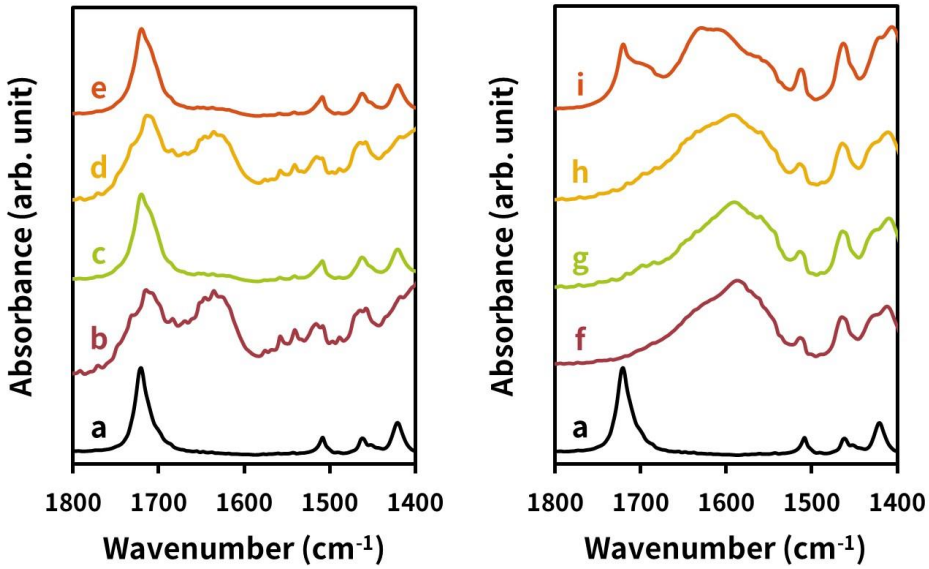

Figure 6. FT-IR spectra of (a) IB, (b) 10 wt% IB/SBA-15-ads, (c) 50 wt% IB/SBA-15-imp, (d) 10 wt% IB/SBA-15-phy, (e) 50 wt% IB/SBA-15-phy, (f) 30 wt% IB/MgO/SBA-15-ads, (g) 50 wt% IB/MgO/SBA-15-imp, (h) 30 wt% IB/MgO/SBA-15-phy, and (i) 50 wt% IB/MgO/SBA-15-phy.

3.6. THz-TDS analyses

As stated above, THz-TDS spectroscopy can be a useful tool for investigating drugs. Pure IB showed characteristic absorption bands in its THz-TDS spectrum, while SBA-15 and MgO did not exhibit any absorption bands (Figure S1). Figure 7 shows the second-order differential THz-TDS spectra. Ten wt% of IB loadings on SBA-15 in the adsorption and physical mixing methods show no IB absorption peaks, as confirmed by the XRD patterns (Figures 2c and e and 7c and e). Therefore, 10 wt% IB content was considered not detectable under the SBA-15 absorption background. As IB content increased to 50 wt%, absorptions at the same positions as pure IB were detected (Figure 7d and f). As mentioned above, 50 wt% IB/SBA-15-imp and 50 wt% IB/SBA-15-phy showed pure IB XRD patterns (Figure 2d and f). Therefore, at higher IB content, IB with a similar chemical state as pure IB would be detectable even with SBA-15.

When using MgO/SBA-15 as a drug carrier, IB sensitivity decreased, compared to that of IB-loaded SBA-15 (Figure 7h–k). Thirty wt% IB/MgO/SBA-15-ads and 50 wt% IB/MgO/SBA-15-imp did not show IB absorption (Figure 7h and i). The former did not show the IB XRD peaks, while the latter showed the XRD pattern which was different from that of pure IB (Figure 2h and i). Hence, the dispersion state and the crystal structure of IB species seemed to greatly influence their sensitivity

to THz-TDS spectroscopy. Although 30 wt% IB/MgO/SBA-15-phy only showed a negligible absorption signal, 50 wt% IB/MgO/SBA-15-phy showed absorption signals similar to pure IB (Figure 7j and k). Therefore, it was confirmed that IB species absorption in the THz-TDS measurement was roughly correlated with the peak intensities of the pure IB XRD pattern and the FT-IR absorption at 1720 cm^{-1} due to the carboxyl C=O stretching vibration (Figures 2 and 6). These observed sensitivity change could be used to evaluate the interaction between a drug and an inorganic carrier, which could enhance the controlled drug release ability [3].

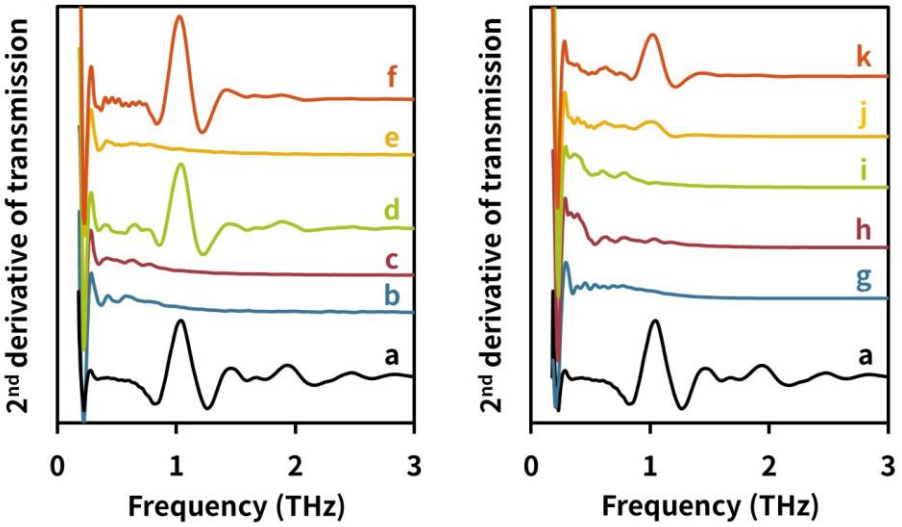

Figure 7. Second-order derivative THz-TDS spectra of (a) IB, (b) SBA-15, (c) 10 wt% IB/SBA-15-ads, (d) 50 wt% IB/SBA-15-imp, (e) 10 wt% IB/SBA-15-phy, (f) 50 wt% IB/SBA-15-phy, (g) MgO/SBA-15, (h) 30 wt% IB/MgO/SBA-15-ads, (i) 50 wt% IB/MgO/SBA-15-imp, (j) 30 wt% IB/MgO/SBA-15-phy, and (k) 50 wt% IB/MgO/SBA-15-phy.

The physical and chemical properties of a drug such as crystallinity, crystal phase, drug dispersion, and interaction with a carrier, can greatly influence the performance of DDSs. Acid-base interactions between a drug and carrier are key factors in controlling drug release by the present drug carrier system and various DDSs [3–5]. Hence, this study demonstrated that THz-TDS spectroscopy can be a rapid and non-destructive tool to investigate the above crucial physical and chemical properties.

4. Conclusions

MgO/SBA-15 was synthesized by a facile one-pot synthesis method, retaining the ordered mesopores. TG-DTAs revealed that IB adsorption capacity was improved from 10 wt% to 30 wt% by modifying SBA-15 with MgO. This improvement could be due to basicity enhancement, which was evaluated in the CO_2-TPD measurements. After loading IB on SBA-15 and MgO/SBA-15 in the adsorption, impregnation, and physical mixing methods, IB-loaded SBA-15s and MgO/SBA-15s were characterized using various techniques. The XRD patterns at low diffraction angles indicated that the ordered mesoporous structures were maintained even after loading IB. Additionally, MgO modification altered or weakened pure IB XRD intensities at high diffraction angles. In the adsorption method, the pure IB XRD pattern was not detected for 30 wt% IB/MgO/SBA-15-ads. Moreover, unlike IB/MgO/SBA-15-imp and IB/MgO/SBA-15-phy, relatively large aggregates of IB and MgO/SBA-15 were not observed for the 30 wt% IB/MgO/SBA-15-ads. Therefore, MgO modification would be effective in dispersing more IB and lowering crystallinity. The higher oxidative decomposition temperature of IB loaded on MgO/SBA-15 and COOH absorption band shifts, which were confirmed using TG-DTA and FT-IR, is indicative of MgO-modified surface and IB interaction. The THz-TDS investigations suggested that MgO modification influenced sensitivity to IB. It was

confirmed that IB species absorption in the THz-TDS investigations roughly correlated with the peak intensities of the pure IB XRD pattern and the FT-IR absorption at 1720 cm^{-1} due to the carboxyl C=O stretching vibration. Therefore, this study demonstrated that THz-TDS spectroscopy could be a rapid and non-destructive tool to investigate the physical and chemical properties of various DDSs.

Supplementary information

IB, SBA-15, and MgO THz-TDS spectra are available in the supplementary material.

Funding

This research received no external funding.

Conflicts of Interest

The author declares no conflicts of interest.

References

1. Florek, J.; Caillard, R.; Kleitz, F. Evaluation of mesoporous silica nanoparticles for oral drug delivery – current status and perspective of MSNs drug carriers. *Nanoscale* **2017**, *9*, 15252–15277. https://doi.org/10.1039/C7NR05762H
2. Zhao, D.; Feng, J.; Huo, Q.; Melosh, N.; Fredrickson, G.H.; Chmelka, B.F.; Stucky, G.D. Triblock copolymer syntheses of mesoporous silica with periodic 50 to 300 angstrom pores. *Science* **1998**, *279*, 548–552. https://doi.org/10.1126/science.279.5350.548
3. Shen, S.; Chow, P.S.; Chen, F.; Tan, R.B.H. Submicron particles of SBA-15 modified with MgO as carriers for controlled drug delivery. *Chem. Pharm. Bull.* **2007**, *55*, 985–991. https://doi.org/10.1248/cpb.55.985
4. Vavsari, V.F.; Ziarani, G.M.; Badiei, A. The role of SBA-15 in drug delivery. *RSC Adv.* **2015**, *5*, 91686–91707. https://doi.org/10.1039/C5RA17780D
5. Alexa, I.F.; Ignat, M.; Popovici, R.F.; Timpu, D.; Popovici, E. In vitro controlled release of antihypertensive drugs intercalated into unmodified SBA-15 and MgO modified SBA-15 matrices. *Int. J. Pharm.* **2012**, *436*, 111–119. https://doi.org/10.1016/j.ijpharm.2012.06.036
6. Zheng, X.; Feng, S.; Wang, X.; Shi, Z.; Mao, Y.; Zhao, Q.; Wang, S. MSNCs and MgO-MSNCs as drug delivery systems to control the adsorption kinetics and release rate of indometacin. *Asian J. Pharm. Sci.* **2019**, *14*, 275–286. https://doi.org/10.1016/j.ajps.2018.08.004
7. Lee, H.V.; Juan, J.C.; Taufiq-Yap, Y.H.; Kong, P.S.; Rahman, N.A. Advancement in heterogeneous base catalyzed technology: An efficient production of biodiesel fuels. *J. Renew. Sustain. Energy* **2015**, *7*, 32701–32746. https://doi.org/10.1063/1.4919082
8. Barros, S.D.T.; Coelho, A.V.; Lachter, E.R.; San Gil, R.A.S.; Dahmouche, K.; Pais da Silva, M.I.; Souza, A.L.F. Esterification of lauric acid with butanol over mesoporous materials. *Renew. Energy* **2013**, *50*, 585–589. https://doi.org/10.1016/j.renene.2012.06.059
9. Huang, B.; Li, X.; Ji, S.; Lang, B.; Habimana, F.; Li, C. Effect of MgO promoter on Ni-based SBA-15 catalysts for combined steam and carbon dioxide reforming of methane. *J. Nat. Gas Chem.* **2008**, *17*, 225–231. https://doi.org/10.1016/S1003-9953(08)60055-9
10. Scholz, J.; Walter, A.; Hahn, A.H.P.; Ressler, T. Molybdenum oxide supported on nanostructured MgO: Influence of the alkaline support properties on MoO_x structure and catalytic behavior in selective oxidation. *Micropor. Mesopor. Mater.* **2013**, *180*, 130–140. https://doi.org/10.1016/j.micromeso.2013.05.032
11. Hu, L.; Yang, F.; Lu, W.; Hao, Y.; Yuan, H. Heterogeneous activation of oxone with CoMg/SBA-15 for the degradation of dye Rhodamine B in aqueous solution. *Appl. Catal. B-Environ.* **2013**, *134–135*, 7–18. https://doi.org/10.1016/j.apcatb.2012.12.028
12. Wang, N.; Yu, X.; Shen, K.; Chu, W.; Qian, W. Synthesis, characterization and catalytic performance of MgO-coated Ni/SBA-15 catalysts for methane dry reforming to syngas and hydrogen. *Int. J. Hydrogen Energ.* **2013**, *38*, 9718–9731. https://doi.org/10.1016/j.ijhydene.2013.05.097
13. Chiou, J.Y.Z.; Yang, S.-Y.; Lai, C.-L.; Kung, H.-Y.; Tang, C.-W.; Wang, C.-B. Steam reforming of ethanol over CoMg/SBA-15 catalysts. *Mod. Res. Catal.* **2013**, *2*, 13–21. http://dx.doi.org/10.4236/mrc.2013.22A003
14. Li, B.; Xu, Z.; Jin, F.; Luo, S.; Chu, W. Facile one-pot synthesized ordered mesoporous Mg-SBA-15 supported PtSn catalysts for propane dehydrogenation. *Appl. Catal. A-Gen.* **2017**, *533*, 17–27. https://doi.org/10.1016/j.apcata.2016.12.026
15. Fu, X.; Zhao, N.; Li, J.; Xiao, F.; Wei, W.; Sun, Y. Carbon dioxide capture by MgO-modified MCM-41

materials. *Adsorpt. Sci. Technol.* **2009**, *27*, 593–601. https://doi.org/10.1260/0263-6174.27.6.593

16. Liu, Q.; Ma, J.; Zhou, Y.; Wang, T. Synthesis of MgO-modified mesoporous silica and its adsorption performance toward CO_2. *Wuhan Univ. J. Nat. Sci.* **2014**, *19*, 111–116. https://doi.org/10.1007/s11859-014-0986-4

17. Wang, R.; Liu, X.; He, Y.; Yuan, Q.; Li, X.; Lu, G.; Zhang, T. The humidity-sensitive property of MgO-SBA-15 composites in one-pot synthesis. *Sensor. Actuat. B-Chem.* **2010**, *145*, 386–393. https://doi.org/10.1016/j.snb.2009.12.025

18. Anbia, M.; Neyzehdar, M.; Dehghan, R. A humidity sensor based on MgO-MCM-41 nanoporous silica. *J. Porous Mat.* **2017**, *20*, 217–225. https://doi.org/10.1615/JPorMedia.v20.i3.30

19. Wei, Y.L.; Wang, Y.M.; Zhu, J.H.; Wu, Z.Y. In-situ coating of SBA-15 with MgO: Direct synthesis of mesoporous solid bases from strong acidic systems. *Adv. Mater.* **2003**, *15*, 1943–1945. https://doi.org/10.1002/adma.200305803

20. Wang, Y.M.; Wu, Z.Y.; Wei, Y.L.; Zhu, J.H. In situ coating metal oxide on SBA-15 in one-pot synthesis. *Micropor. Mesopor. Mater.* **2005**, *84*, 127–136. https://doi.org/10.1016/j.micromeso.2005.05.024

21. Ehiro, T.; Katagiri, K.; Yamaguchi, S.; Yoshioka, Y. Ficile synthesis of MgO-modified mesoporous silica and its application to a CoMo-based ammonia decomposition catalyst. *J. Ceram. Soc. Jpn.* **2020**, *128*, 84–91. https://doi.org./10.2109/jcersj2.19182

22. Manzano, M.; Aina, V.; Arean, C.O.; Balas, F.; Cauda, V.; Colilla, M.; Delgado, M.R.; Vallet-Regi, M. Studies on MCM-41 mesoporous silica for drug delivery: Effect of particle morphology and amine functionalization. *Chem. Eng. J.* **2008**, *137*, 30–37. https://doi.org/10.1016/J.CEJ.2007.07.078

23. Kubo, S.; Kosuge, K. Salt-induced formation of uniform fiberlike SBA-15 mesoporous silica particles and application to toluene adsorption. *Langmuir* **2007**, *23*, 11761–11768. https://doi.org/10.1021/la701556y

24. Brunauer, S.; Emmett, P.H.; Teller, E. Adsorption of gases in multimolecular layers. *J. Am. Chem. Soc.* **1938**, *60*, 309−319. https://doi.org/10.1021/ja01269a023

25. Tita, B.; Fulias, A.; Stefănescu, M.; Marian, E.; Tita, D. Kinetic study of decomposition of ibuprofen under isothermal conditions. *Rev. Chim. (Bucharest)* **2011**, *62*, 216–221.

Supplementary Material

1. THz-TDS analyses

MgO was prepared by calcining $Mg(OAc)_2 \cdot 4H_2O$ at 823 K for 3 h. The crystal structure of the obtained sample was indexed to MgO using XRD. THz-TDS measurements were performed at 297 K on a Tera Prospector (Nippo Precision Co., Ltd.). Before the measurements, 0.05 g of IB, diluted with polyethylene powder (Sigma-Aldrich Japan, Inc.), 0.1 g of SBA-15, and 0.1 g of MgO, was pelletized to form discs with 15 mm diameter. The optical system was operated in a dry air atmosphere to avoid water absorption signature.

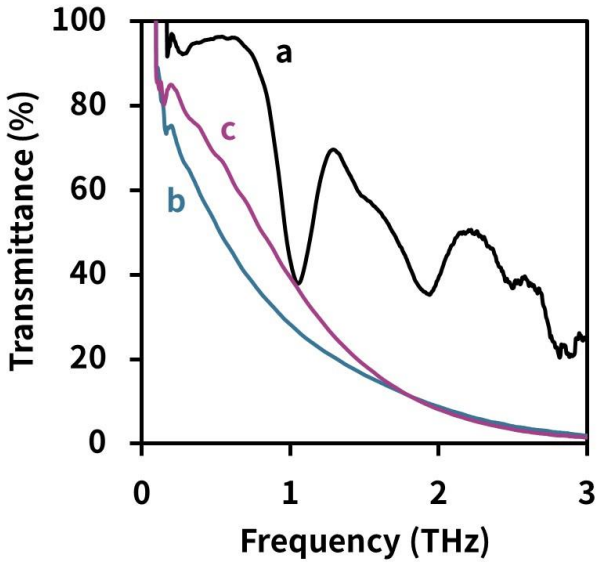

Figure S1. THz-TDS spectra of (a) IB, (b) SBA-15, and (c) MgO.